ISBN: 978-3-95450-232-5 ISSN: 2673-7000 doi:10.18429/JACoW-NAPAC2022-MOYE6

SPIN POLARIZED ELECTRON PHOTOEMISSION AND DETECTION STUDIES

A. C. Rodriguez Alicea, University of Puerto Rico - Mayaguez, Mayaguez, PR, USA
O. Chubenko, S. Karkare, Arizona State University, Tempe, AZ, USA
R. Palai, University of Puerto Rico - Rio Piedras, San Juan, PR, USA
L. Cultrera, Brookhaven National Laboratory, Upton, NY, USA

Abstract

The experimental investigation of new photocathode materials is time-consuming, expensive, and difficult to accomplish. Computational modelling offers fast and inexpensive ways to explore new materials, and operating conditions, that could potentially enhance the efficiency of polarized electron beam photocathodes. We report on Monte-Carlo simulation of electron spin polarization (ESP) and quantum efficiency (QE) of bulk GaAs at 2, 77, and 300 K using the data obtained from Density Functional Theory (DFT) calculations at the corresponding temperatures. The simulated results of ESP and QE were compared with reported experimental measurements, and showed good agreement at 77 and 300 K.

INTRODUCTION

Photocathodes are very important in accelerator physics, they generate high brightness spin polarized electron beams that will allow scientist to unravel mysteries about the fundamental particle interactions and cosmology history [1]. Spin polarized electron beams can be characterized by quantum efficiency (QE), electron spin polarization (ESP), and lifetime. GaAs photocathodes as a source for spin polarized electrons was first proposed in 1974, and shortly after experiments obtained 40% ESP and 10% QE from bulk crystals of the material using circularly polarized light [2]. Due to the degenerate light-hole and heavy-hole band states in the $P_{3/2}$ valence band, the theoretical limit of ESP for these bulk GaAs sources was about 50%. To overcome this problem, strained layers (SL) of GaAs alloys have been studied, since the pseudomorphic strain alleviates the electron level's degeneracy limitation. Although the SL enabled measured ESP over 90%, its QE drastically dropped to below 1% [3]. Deploying a distributed Bragg reflectors (DBR) allows the material to retain more light, and increases the QE to around 10% [4]. Several other approaches have been explored, but desirable beam properties, high ESP with high QE and long lifetime, have not been achieved [5], which warrants further investigation beyond III-V semiconductors as photocathodes.

The experimental investigation of new photocathode materials is time-consuming, expensive, and difficult to accomplish. Computational modeling offers an inexpensive way to explore new materials and operating conditions that could potentially enhance the efficiency of GaAs based photocathodes, with relatively more ease and at much lower cost. The main objective of the present work is to develop a framework where the *ab-initio* numerical calculation data of electronic band structures can be used to provide inputs to a Monte Carlo (MC) simulations, that have successfully reproduced experimental observations of QE and ESP in bulk GaAs [6], in order to predicts the photoemission from novel materials. The QE and ESP strongly depend on the experimental conditions such as, photon energy and temperature. The present work investigate how these parameters can change with temperature for bulk GaAs and compare the results with experimental observations from Liu *et al.* [7]. Once the framework has been completed for this material, we can explore new ones and screen possible candidates for experimental studies, making the overall process of research and development more feasible.

CALCULATION DETAILS

Density functional theory (DFT) calculations can predict various macroscopic properties of materials, taking as input only the basic crystal structure. For mott insulators, in which the correlation and spin attributes of the material makes their electrical properties deviate from classical predictions, DFT calculations tend to over-delocalize valence electrons and to over-stabilize conduction bands, resulting in smaller intrinsic energy gaps compared to what is observed experimentally. The Hubbard correction takes into account the energy contributions of spin correlations and enables for more precise predictions for such materials [8]. This approach has been implemented in this work using *Quantum Espresso* program package to obtain accurate prediction of GaAs electronic band structure, dielectric permittivity, and phonon dispersion of GaAs [9].

All the energy approximations used for DFT calculation are dependent on the lattice structure, which is affected by temperature variations. To compensate for the temperature variation, we changed the lattice constant of the crystal following the empirical formula $a = a_o + 7.3321 \times 10^{-5}(T)$, where a_o is the optimal lattice for 0 K, found to be 10.4549 a. u. with the relaxation calculation [10]. We selected 2, 77 and 300 K for the representative temperatures of liquid Helium, liquid Nitrogen and room temperature respectively.

The formulas used for the calculation of different parameters are as follow; from the energy in k-space diagrams (band structure) we can estimate the effective masses using the relation $1/m^* = d^2E/dk^2 m_0/\hbar^2$ [11]. The selected path goes through the three symmetry points in the Brillouin zone, L, X, and Γ, in three different directions to give the effective masses as harmonic average, $m^* = 3 \cdot (\frac{1}{m_x^*} + \frac{1}{m_y^*} + \frac{1}{m_z^*})^{-1}$ [12].

ISBN: 978-3-95450-232-5 ISSN: 2673-7000 doi:10.18429/JACoW-NAPAC2022-MOYE6

The effective masses were calculated for the electron in the Conduction band (CB) at *X*, Γ and *L*-valley, and for the split-off (SO), heavy-hole (HH) and light-hole (LH) band at the Γ-valley. Non-parabolicities are obtained following the equation $\alpha_i = (1 - m_0^*/m_0)^2/E_g$ for every i valley mentioned before [13]. The energy splittings are also calculated from the band diagrams, measuring directly the differences between corresponding valleys. The index of refraction and extinction coefficient were obtained from the real and imaginary parts of the dielectric permittivity calculation using equations $n = \sqrt{(\epsilon_R + \sqrt{\epsilon_i^2 + \epsilon_R^2})/2}$ and $k = \sqrt{(-\epsilon_R + \sqrt{\epsilon_i^2 + \epsilon_R^2})/2}$, respectively. The absorption coefficient is obtained as $\alpha = \frac{4 \cdot \pi \cdot k}{\lambda}$, where λ is the wavelength [14]. Finally, intervalley scattering phonon energies, and the polar optical phonon energy, were calculated from the phonon dispersion relation as average of all the possible scattering mechanisms. All the parameters obtained from DFT calculations at 2, 77, and 300 K are given in Table 1, with reported data at 300 K from Chubenko *et al.* [6].

Table 1: Table with All the Parameters at Each Temperature and as Expected from Chubenko's Simulation [6]

Parameter	2 K	77 K	300 K	Ref. 300 K
Electron's effective mass (m*)				
CB - X	0.294	0.282	0.283	0.58
CB - Γ	0.0687	0.0683	0.0661	0.063
CB - L	0.130	0.130	0.129	0.22
HH	0.368	0.368	0.374	0.50
LH	0.0801	0.0804	0.0785	0.088
SO	0.118	0.117	0.114	0.15
Energy gap (eV)				
Intrinsic	1.52	1.51	1.42	1.42
Split-off	0.362	0.361	0.360	0.332
Splitting energy (eV)				
Γ - L	0.008	0.024	0.034	0.284
Γ - X	0.315	0.330	0.381	0.476
Nonparabolicity factor (eV^{-1})				
Γ	0.571	0.574	0.611	0.61
L	0.498	0.500	0.532	0.461
X	0.328	0.341	0.360	0.204
Optical parameters (ϵ_0)				
H.f. dielectric	11.40	11.43	11.49	10.92
Static dielectric	11.79	11.82	11.90	12.90
Intervalley scattering phonon energy (meV)				
Γ → L	31.8	31.7	29.7	27.8
Γ → X	31.1	30.9	29.7	29.9
L→ L	31.8	31.7	29.7	29
L → X	31.5	31.3	29.7	29.3
X → X	31.8	31.7	29.7	29.9
Other				
Polar optical phonon energy (meV)	35.0	34.9	34.1	35.36
Crystal density ($kg \cdot m^{-3}$)	5640	5632	5605	5360
Sound velocity ($m \cdot s^{-1}$)	5127	5125	5004	5240

RESULTS AND DISCUSSION

DFT Calculations

The approach for the electronic structure was based on the Plane Augmented Wave method with fully-relativistic calculations [15]. We observed that the Hubbard contribution of As has significant effects on band gap E_g, and consequently in the effective mass, while Ga barely caused any changes in the E_g nor the effective masses. For such reason, the Hubbard correction was only applied to As. Figure 1(a) shows the calculated band structure of GaAs through the path *X*-Γ-*L* at different temperatures. The corrected energy gap was found to be 1.52, 1.51, and 1.42 eV at 2, 77, and 300 K, respectively. The band diagram accurately reflects the direct band gap of GaAs at Γ-valley. However, the energy difference between the Γ and *L*-valley is roughly one order of magnitude smaller than what we expected, while the energy splitting between the Γ and *X*-valley is a little above the anticipated value. On the other hand, the effective masses as well as the non-parabolocity factors are fairly in agreement with anticipated values, as they maintained their relative values. We observed that non-parabolicity as well as the energy splittings between conduction band minimum (CBM) and valence band maximum (VBM) tend to increase with temperature, while the effective masses tend to decrease, with the exception of the effective mass for the heavy hole (HH) band.

The phonon dispersion calculation was carried out using a non-local norm-conserving pseudopotential from the *Quantum Espresso* pseudopotential library. Figure 1(b) shows phonon dispersion of GaAs at the high symmetry points with normal modes of all branches. As can be seen, there is a splitting of transverse and longitudinal phonon modes at $k \neq 0$. At the Γ point, which corresponds to $k = 0$, the acoustic branches (transverse acoustic (TA) and longitudinal acoustic (LA)) show linear dependence, while the longitudinal optical (LO) phonons have higher energy compared to the transverse optical (TO) phonons, as expected [16]. The scattering phonon energy shows minimal decreases with increasing temperature.

Finally, the complex dielectric permittivity was calculated using a the same norm-conserving method as the phonon calculations. The absorption and reflection spectra as a function of incident photon energy, Figs. 2(a) and 2(b) respectively, shows increases in intrinsic absorption and reflection with photon energy and corresponding temperature.

Monte Carlo Simulations

In order to predict the ESP and QE of GaAs, MC simulations using Chubenko *et al.* [6] code were performed using

ISBN: 978-3-95450-232-5 ISSN: 2673-7000 doi:10.18429/JACoW-NAPAC2022-MOYE6

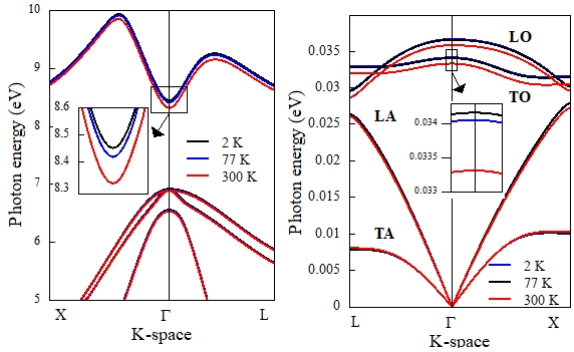

(a) (b)

Figure 1: 1(a) Band structure obtained from DFT near the fermi level at the different symmetry points and varying temperatures. 1(b) Phonon dispersion obtained from DFT at the different symmetry points and temperatures. Both figures include a zoom for better visualization of the effects temperature has on each graph.

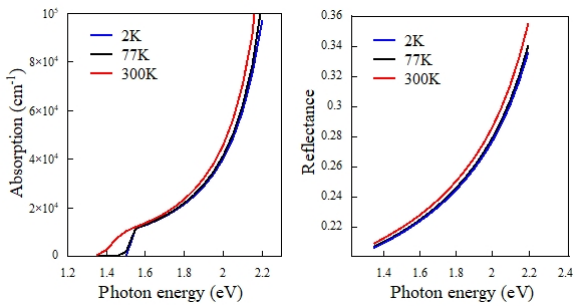

(a) (b)

Figure 2: 2(a) Absorption and 2(b) reflectance as a function of photon energies as calculated from DFT complex dielectric calculation at different temperatures.

the physical parameters from Table 1, obtained from DFT calculations at the temperatures 2, 77, and 300 K. Figures 3(b) and 3(a) show the MC simulation results. The simulation data were compared with the reported experimental results by Liu *et al.* [7]. As can be seen, the MC simulated data of ESP GaAs qualitatively agrees with the reported results at both 77 K and 300 K. There are not data available at 2 K and the simulation results appear to be largely scattered. We are still investigating and bench marking the DFT-MC framework against the available experimental data. Our DFT simulations were performed for intrinsic materials, and because of that we relied on a expression for the location of the Fermi level that was derived to be used at room temperature [6]. Similarly the correction introduced in the band gap calculated with DFT to take into account the doping density was not derived for use at very low temperatures [6].

CONCLUSION

We have successfully simulated the ESP and QE of GaAs by combining MC simulations using the data obtained from DFT calculations at different temperatures. The simulated

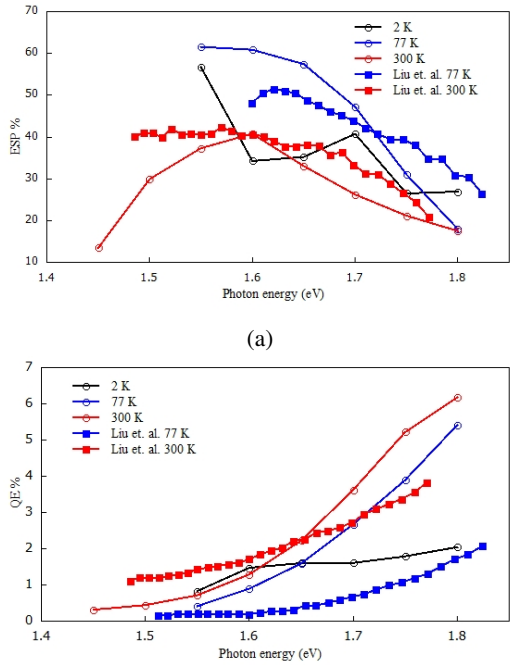

(a)

(b)

Figure 3: Results from the MC simulation for the polarized electron photoemission at different temperatures with reference experimental measurements from Liu *et al.* [7].

results of ESP and QE showed good qualitative agreement with experimental reports at 77 and 300 K. At 2 K, there appears to be a deviation from the expected trend line, but there is no experimental data from which we can make conclusive statements. We are still working to improve our modeling and achieve better agreement with available experimental data. As the number of electron guns intended to operate with photocathodes held at cryogenic temperatures increase, it is becoming more and more important to characterize photoemission properties at low temperatures. These studies offer insight into the performance that known material will have when operated in uncommon experimental conditions and can be used to enhance the quality of the prediction of numerical simulation based on a DFT-MC framework that can lead to identify new photocathodes candidates for the production of spin polarized electron beams.

ACKNOWLEDGEMENTS

This project was supported in part by the Brookhaven National Laboratory (BNL), Instrumentation Division and the U.S. Department of Energy, Minority Serving Institutions under the Fellowship Program for Research Excellence in Nuclear Physics. The authors also thank the Center for Bright Beams, NSF award PHY-1549132.

REFERENCES

[1] A. Accardi *et al.*, "Electron ion collider: The next QCD frontier - understanding the glue that binds us all," *arXiv preprint*, 2012. doi:10.48550/arXiv.1212.1701

ISBN: 978-3-95450-232-5 ISSN: 2673-7000 doi:10.18429/JACoW-NAPAC2022-MOYE6

[2] D. T. Pierce *et al.*, "The GaAs spin polarized electron source," *Review of Scientific Instruments*, vol. 51, no. 4, pp. 478–499, 1980. doi:10.1063/1.1136250

[3] T. Maruyama, E. L. Garwin, R. Prepost, G. H. Zapalac, J. S. Smith, and J. D. Walker, "Observation of strain-enhanced electron-spin polarization in photoemission from InGaAs," *Physical Review Letters*, vol. 66, no. 18, pp. 2376–2379, 1991. doi:10.1103/PhysRevLett.66.2376

[4] W. Liu *et al.*, "Record-level quantum efficiency from a high polarization strained GaAs/GaAsP superlattice photocathode with distributed Bragg reflector," *Applied Physics Letters*, vol. 109, no. 25, p. 252 104, 2016. doi:10.1063/1.4972180

[5] J. K. Bae, A. Galdi, L. Cultrera, F. Ikponmwen, J. Maxson, and I. Bazarov, "Improved lifetime of a high spin polarization superlattice photocathode," *Journal of Applied Physics*, vol. 127, no. 12, p. 124 901, 2020. doi:10.1063/1.5139674

[6] O. Chubenko *et al.*, "Monte Carlo modeling of spin-polarized photoemission from p-doped bulk GaAs," *Journal of Applied Physics*, vol. 130, no. 6, p. 063 101, 2021. doi:10.1063/5.0060151

[7] W. Liu, M. Poelker, X. Peng, S. Zhang, and M. Stutzman, "A comprehensive evaluation of factors that influence the spin polarization of electrons emitted from bulk GaAs photocathodes," *Journal of Applied Physics*, vol. 122, p. 035 703, 2017. doi:10.1063/1.4994306

[8] M. Cococcioni, "The LDA + U approach : A simple Hubbard correction for correlated ground states," 2012.

[9] P. Giannozzi *et al.*, "QUANTUM ESPRESSO: A modular and open-source software project for quantum simulations of materials," *Journal of Physics: Condensed Matter*, vol. 21, no. 39, p. 395 502, 2009. doi:10.1088/0953-8984/21/39/395502

[10] H. Jappor, "Band-structure calculations of GaAs within semiempirical large unit cell method," *European Journal of Scientific Research*, vol. 59, pp. 264–275, 2011.

[11] O. Badami *et al.*, "Comprehensive Study of Cross-Section Dependent Effective Masses for Silicon Based Gate-All-Around Transistors," *Applied Sciences*, vol. 9, no. 9, 2019. doi:10.3390/app9091895

[12] M. A. Green, "Intrinsic concentration, effective densities of states, and effective mass in silicon," *Journal of Applied Physics*, vol. 67, no. 6, pp. 2944–2954, 1990. doi:10.1063/1.345414

[13] D. Vasileska and S. Goodnick, *Computational Electronics*. Morgan & Claypool Publishers, 2006. https://books.google.com/books?id=DBPnzqy5Fd8C

[14] M. S. Dresselhaus, *Solid state physics part II optical properties of solids*.

[15] A. Dal Corso, "Pseudopotentials periodic table: From H to Pu," *Computational Materials Science*, vol. 95, pp. 337–350, 2014. doi:10.1016/j.commatsci.2014.07.043

[16] L. Lindsay, D. A. Broido, and T. L. Reinecke, "Ab initio thermal transport in compound semiconductors," *Physical Review B*, vol. 87, no. 16, p. 165 201, 2013. doi:10.1103/PhysRevB.87.165201